Journal of Sound and Vibration (1997) **200**(5), 701–719

NOISE FROM SUPERSONIC COAXIAL JETS, PART 3: INVERTED VELOCITY PROFILE

M. D. Dahl

National Aeronautics and Space Administration, Lewis Research Center, Cleveland, OH 44135, *U.S.A.*

AND

P. J. Morris

Department of Aerospace Engineering, The Pennsylvania State University, University Park, PA 16802, *U.S.A.*

(*Received* 5 *February* 1996, *and in final form* 19 *August* 1996)

The instability wave noise generation model is used to study the instability waves in the two shear layers of an inverted velocity profile, supersonic, coaxial jet and the noise radiated from the dominant wave. The inverted velocity profile jet has a high speed outer stream surrounding a low speed inner stream and the outer shear layer is always larger than the inner shear layer. The jet mean flows are calculated numerically. The operating conditions are chosen to exemplify the effect of the coaxial jet outer shear layer initial spreading rates. Calculations are made for the stability characteristics in the coaxial jet shear layers and the noise radiated from the instability waves for different operating conditions with the same total thrust, mass flow and exit area as a single reference jet. Results for inverted velocity profile jets indicate that relative maximum instability wave amplitudes and far field peak noise levels can be reduced from that of the reference jet by having higher spreading rates for the outer shear layer, low velocity ratios, and outer streams hotter than the inner stream.

1. INTRODUCTION

A method to modify the generation of mixing noise in supersonic axisymmetric jets is to replace the single stream jet by a dual stream, coaxial jet. These jets are classified as having a normal velocity profile (NVP) if the inner stream velocity is higher than the outer stream velocity at the nozzle exit. If the initial inner stream velocity is less than the initial outer stream velocity, the coaxial jet is classified as having an inverted velocity profile (IVP). In addition, the two jet streams may have different initial temperatures. This paper concentrations on IVP supersonic jets. NVP supersonic jets are discussed in a previous paper (Part 2 [1]).

In this paper the results are described from an analysis of the effects of different jet operating conditions on the ability of the jet to generate mixing noise. The analysis is based on recent theories for supersonic jet noise that use the concepts of linear instability wave theory to predict radiated noise. These theories have established that instability waves are the dominant source of mixing noise radiating into the downstream arc of a supersonic jet. Previously applied to single stream supersonic jets with a single shear layer, the analysis is now applied to a dual stream supersonic jet with two initial shear layers that eventually merge into a single shear layer downstream. A known mean flow is required to complete

0022–460X/97/100701 + 19 $25.00/0/sv960725

the analysis and Part 1 of this paper [2] described a numerical scheme to calculate the mean flow properties for any set of IVP coaxial jet operating conditions.

1.1. IVP COAXIAL JET NOISE

Early studies of by-pass jet engines showed that they had reduced noise levels compared to a turbojet engine at the same mass flow. In addition to the lower velocities in a by-pass engine, measured noise reductions were shown to be due to the decrease in the mean shear of the combined flow [3]. This apparent noise reduction benefit of two stream coaxial jets operating in subsonic conditions was convincing enough to cause researchers to look for similar benefits under supersonic conditions. Dosanjh and his colleagues conducted an extensive experimental study of supersonic coaxial jets that focused on IVP operating conditions as a means of reducing shock noise. Using small scale nozzles, they optically observed, measured and documented the existence of a minimum noise operating condition for shock containing IVP coaxial jets [4–6]. It initially appeared that the overall noise reduction was primarily due to a decrease in shock associated noise. However, in further studies on a larger scale coaxial jet nozzle, noise reductions were measured at all frequencies and at all angles [7–9]. This meant that not only was shock noise—which dominates in the upstream direction—reduced but also that mixing noise—which dominates in the downstream direction—was reduced. It was also found that directivity patterns could be changed by the choice of pressure and temperature operating conditions.

Tanna *et al*. [10] conducted measurements of shock-free coaxial jets with inverted velocity profiles to study the effects of profile shaping in jet mixing noise. In addition, care was taken in choosing initial velocity and temperature conditions along with the exit area in order to compare results on a constant thrust, mass flow and exit area basis to a fully mixed equivalent single jet or reference jet. They found that high frequency noise increased at all angles and that low frequency noise decreased at angles closer to the jet exit axis. These changes were relative to the reference jet and they became larger as the velocity ratio increased above 1. Far field spectra remained largely unaffected by higher temperature ratios for a coaxial jet with both velocities the same. Since the far field spectra were peaking at the lower frequencies, the overall sound pressure levels were quieter for $U_2/U_1 > 1$ at smaller angles and noisier at 90 degrees. The higher frequency noise was generated primarily from the outer shear layer before the streams merged. As U_2/U_1 increased, the outer shear layer had a larger velocity difference to ambient, resulting in higher eddy convection velocities, higher source velocities and more noise. Conversely, the lower frequency noise was generated downstream of merging where the velocities were lower, resulting in less noise. It has also been concluded that the rapid decay of the maximum mean velocity in inverted velocity profile jets is a prominent reason for noise reduction in IVP jets compared to the reference jet [11].

The experimental work on coaxial jets was continued into the supersonic regime using converging nozzles that were operated above critical pressure ratios, resulting in underexpanded, shock-containing jet flows [12]. A minimum noise condition, based on overall sound pressure level measurements at upstream angles where shock associated noise dominates, was found for a fixed outer nozzle pressure ratio above critical. This occurred when the inner nozzle pressure ratio was slightly above critical, at about 1·9. With the shock associated noise virtually eliminated, measurements were made of the remaining mixing noise at downstream angles to the jet axis. Test conditions of constant thrust, mass flow and exit area, along with the added condition that the inner stream be slightly supersonic to achieve minimum noise due to shocks, were used to set the coaxial jet initial velocities and temperatures. As was found for shock-free coaxial jets, inverted velocity

profile jets were quieter than the reference jet based on overall sound pressure level measurements at 30 degrees to the jet axis.

1.2. INSTABILITY WAVES IN IVP JETS

In supersonic jets, instability waves have been established as a dominant source of mixing noise. These waves, generated by the instability of the jet shear layer, radiate noise when they have phase velocities that are supersonic relative to ambient conditions. Initially, both shear layers will support growing instability waves. As the shear layers grow and merge together, the growth rates and phase velocities of these instability waves will be modified by this process.

Measurements have been made of the large scale structures or instability waves in subsonic IVP coaxial jets [13, 14]. Using cross-spectral techniques, the phase relationship between fluctuating quantities was measured. The phase relationship in the outer shear layer suggested that convecting large scale structures existed there that were similar to those that exist in single jets. In the inner shear layer, similar phase relationships existed, except with the opposite sign of rotation for the large structures. The outer shear layer vortex sheet rolled up in an outward sense of rotation and the large scale structures joined into larger ones downstream. These outer shear layer structures were convected downstream into the merging and fully developed regions and were not significantly affected by changes in the mean velocity ratio. Conversely, the inner shear layer structures were affected by changing the velocity ratio. As the velocity ratio increased, the growth of the inner shear layer structures were enhanced. Nonetheless, in the spectral measurements, the lower frequency, outer shear layer peak was typically dominant and the inner shear layer peak disappeared as the IVP coaxial jet merged and became fully developed downstream. Similar conclusions were found from a flow visualization study of low speed, incompressible, coaxial jets, that revealed the large scale structures in the two shear layers as the velocity ratio varied between 1 and 2·59 [15].

Following the approach used for single jets with a single shear layer, the local stability characteristics can be calculated in the same manner for the two shear layers in a coaxial jet. Bhat and Seiner [16] made such calculations for an IVP supersonic coaxial jet using a mean flow that was described analytically; however, due to a lack of measured data on the merging of the two streams, the mean flow description only applied in the core region. For the IVP jet with a velocity ratio of 1·91, the outer shear layer stability characteristics were found to be similar to the equivalent single jet stability characteristics. These results were in agreement with the trends observed from the measured low speed coaxial jet data discussed above. Since the mean flow was not known beyond the end of the potential core region, the complete growth and decay of the instability waves could not be obtained.

1.3. THEORETICAL CONSIDERATIONS

When the supersonic jet is perfectly expanded, the instability waves generated noise that has a radiation pattern with a dominant peak in the downstream arc of the jet. In Part 2 of this paper [1], we developed a prediction scheme that could analyze the mixing noise, where it dominates, from supersonic coaxial jets. Assuming the jet to be perfectly expanded simplified the analysis and allowed the study to concentrate on exit velocity profile shaping as a means further to reduce the mixing noise.

The analysis to predict the noise radiated to the far field is based on the determination of the axial growth and decay of the instability wave in the jet shear layer. In order to complete the analysis, the mean flow properties are needed. In Part 1 of this paper [2], we describe the numerical prediction method for the mean flow development. This provides an efficient method to obtain the mean flow for various operating conditions. An outline

of the analysis to calculate the evolution of instability waves and their radiated noise was presented in Part 2 of this paper [1]. Here, in this part of the paper, we give for reference the equations used directly to calculate the instability wave characteristics and the radiated noise.

A parametric study of supersonic IVP coaxial jets has been conducted using our analytical and numerical analysis. We chose a reference single stream jet with operating conditions that would be typical for a supersonic transport aircraft engine exhaust. From these conditions, we defined the operating conditions for supersonic IVP jets that have the same total thrust, total mass flow and total exit area as the reference jet. The choice of these operating conditions was based on an analysis of the initial spreading rate of the outer shear layer. The velocity ratio, the density ratio and the area ratio were each varied separately to determine the resulting effect on the maximum amplitudes of the growing instability waves and the relative levels and directivities of the far field radiated noise. A final set of calculations was performed to show the combined effects of changing all three parameters.

2. INSTABILITY WAVES AND RADIATED NOISE

Thin free shear layers that contain an inflection point in the mean velocity profile are inherently unstable even in the absence of viscosity. Initially, an instability wave in the shear layer grows rapidly. As the shear layer grows, the wave growth rate decreases. Eventually, the shear layer is too thick to support unstable waves and the wave amplitude decreases until it disappears. This instability wave process is assumed to be governed by the linearized, inviscid, compressible equations of motion.

For slowly diverging jet flows, two solutions are created that apply to separate but overlapping regions. Following the approach of Tam and Burton [17], the inner region, including the jet flow and the immediate region just outside the jet, has different length scales in the radial and the axial directions that leads to a multiple scales expansion of the governing equations using the small parameter ε. With the fluctuating pressure disturbance given by the expansion

$$p'(r, \theta, x, t) = \sum_{m=0}^{\infty} \delta_m(\varepsilon)\hat{p}_m(r, s) \exp\left[\mathrm{i}(\phi(s)/\varepsilon + n\theta - \omega t)\right], \tag{1}$$

the components of the lowest order set of equations in non-dimensional form are combined to form the compressible Rayleigh equation

$$\frac{\partial^2 \hat{p}_0}{\partial r^2} + \left[\frac{1}{r} + \frac{2\alpha}{\omega - \alpha\bar{u}}\frac{\partial \bar{u}}{\partial r} - \frac{1}{\bar{\rho}}\frac{\partial \bar{\rho}}{\partial r}\right]\frac{\partial \hat{p}_0}{\partial r} + \left[\bar{\rho}M_1^2(\omega - \alpha\bar{u})^2 - \frac{n^2}{r^2} - \alpha^2\right]\hat{p}_0 = 0, \tag{2}$$

where the axial wavenumber α is related to the axial phase function ϕ by $\alpha = \mathrm{d}\phi/\mathrm{d}s$, s is the slow variable to recognize the slow mean flow development in the axial direction $s = \varepsilon x$, n is the azimuthal mode number, and ω is the radian frequency.

In the outer region, which slightly overlaps the inner region, the governing equations control disturbances that are acoustic in nature. These disturbances have the same length scales in all directions; hence, all co-ordinates are treated equally. The solution is obtained by Fourier transforming the outer region governing equations in the axial direction. After considerable algebra, the lowest order outer solution is

$$p'(r, \theta, x, t) = \int_{-\infty}^{\infty} g(\eta) \mathrm{H}_n^{(1)}(\mathrm{i}\lambda(\eta) r)\, \mathrm{e}^{\mathrm{i}\eta x}\, \mathrm{e}^{\mathrm{i}n\theta}\, \mathrm{e}^{-\mathrm{i}\omega t}\, \mathrm{d}\eta, \tag{3}$$

where

$$g(\eta) = \frac{1}{2\pi} \int_{-\infty}^{\infty} \tilde{A}_0(\varepsilon x)\, \mathrm{e}^{\mathrm{i}\phi(\varepsilon x)/\varepsilon}\, \mathrm{e}^{-\mathrm{i}\eta x}\, \mathrm{d}x, \qquad \lambda(\eta) = [\eta^2 - \bar{\rho}_\infty M_1^2(\omega - \eta \bar{u}_\infty)^2]^{1/2}. \tag{4, 5}$$

$\mathrm{H}_n^{(1)}$ is the nth order Hankel function of the first kind.

After the inner and the outer solutions are matched asymptotically in an overlap region, we find that equation (2) has become an eigenvalue problem with solutions only for certain values of the eigenvalue α. We have used a finite difference approximation to discretize the problem. The eigenvalue is found from the resulting diagonal matrix using a Newton–Raphson iteration for refinement.

Since the rate of spread of the jet is slow for high speed jets and ε is very small, $\tilde{A}_0(\varepsilon x)$ in equation (4) is taken to be constant. Furthermore, with $\alpha(x)$ found from the solution of equation (2) at each axial location, the axial phase function is found from $\phi(\varepsilon x)/\varepsilon = \int_0^x \alpha(\chi)\, \mathrm{d}\chi$. We can then solve for $g(\eta)$ in equation (4), the Fourier transform of the instability wave, and subsequently the near field pressure disturbance is found from equation (3). To obtain the pressure in the far field, equation (3) in spherical co-ordinates is approximated by the method of stationary phase. The resulting sound power radiated per unit solid angle is

$$D(\psi) = \tfrac{1}{2}|p'|^2 R^2 = 2|g(\bar{\eta})|^2/[1 - M_\infty^2 \sin^2 \psi]. \tag{6}$$

The stationary point is given by

$$\bar{\eta} = \frac{\bar{\rho}_\infty^{1/2} M_1 \omega \cos \psi}{(1 - M_\infty^2)(1 - M_\infty^2 \sin^2 \psi)^{1/2}} - \frac{\bar{\rho}_\infty M_1^2 \bar{u}_\infty \omega}{1 - M_\infty^2} \tag{7}$$

and ψ is the polar angle.

2.1. COMPARISONS WITH ANALYTICAL STUDIES

The numerical procedures to solve the eigenvalue problem and to calculate the near and far field pressure disturbances are described in Part 2 of this paper [1]. The accuracy of these procedures is also discussed. The numerical calculations of the disturbance quantities and the mean flow calculations described in Part 1 of this paper [2] are designed to use the jet exit operating conditions as the only known inputs into calculating the local stability characteristics and the far field directivity patterns of axisymmetric jets with both single and dual streams. This allows a wider variety of operating conditions to be studied without relying on measured mean flow parameters, especially in the case of supersonic coaxial jets, for which mean flow data are hard to obtain. To validate our procedures, we chose both single axisymmetric jet and coaxial jet cases where both the mean flow was defined and the stability calculations had been completed under supersonic conditions. The results from our stability calculations have been compared with the results from these reference cases, in which the mean flow was represented by analytic functions for the axial velocity and Crocco's relation for the density, an approach typically used in past studies of jet stability characteristics. As shown in Part 2 of this paper [1], both the stability characteristics and the far field directivity patterns that we calculated for a single jet using

a numerically generated mean flow compared favorably with calculated results where the mean flow was described analytically.

Bhat and Seiner [16] developed an analytic model for the initial mean flow of a supersonic IVP jet for the purposes of conducting stability calculations. The two shear layers were modelled separately, resulting in the mean flow being defined only out to the end of the outer potential core. Due to a lack of measured data, the analytic function flow modelling could not be continued into the merging and fully developed flow regions downstream. The mean velocity profiles were defined by half-Gaussian functions and the spreading rates were determined from the Langley curve. Crocco's relation was used to define the mean density profiles. For the stability calculations, the Rayleigh equation was integrated numerically across each shear layer separately, using analytic functions in the regions of constant mean flow properties to define the four boundary conditions. These calculations resulted in local growth rates and phase velocities as a function of axial distance. An example of their results is shown in Figure 1 for an IVP jet with the following operating conditions: $R_2/R_1 = 3{\cdot}0$, $M_1 = M_2 = 1{\cdot}48$, $U_2/U_1 = 1{\cdot}91$, $T_2/T_1 = 3{\cdot}65$, $T_\infty/T_1 = 1{\cdot}35$. Both axisymmetric ($n = 0$) and first helical ($n = 1$) modes are shown for a Strouhal number $fD_1/U_1 = 0{\cdot}2$. The results are plotted against the local shear layer half-width appropriate to the shear layer with which the eigenvalue is identified; either the inner or outer shear layer. For comparison, the results from our stability calculations are shown in the same figure. No attempt was made to match the spreading rate in the numerical mean flow model to the spreading rates used for the analytic function profiles; nonetheless, the numerical results have similar characteristics to the analytic results when plotted versus the local shear layer half-width. Where the shear layers are thin, the growth rates and phase velocities are almost identical. The primary differences that occur downstream can be attributed to the differences in the profile shapes of the shear layers. The results shown in Figure 1 for an IVP jet provide a validation of our procedure for stability calculations in coaxial jets.

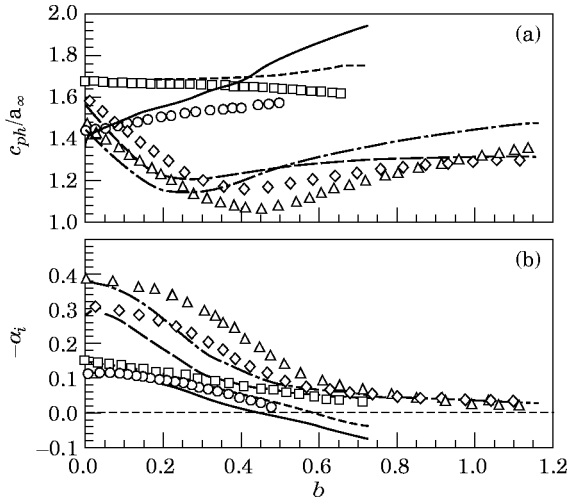

Figure 1. Stability characteristics of an IVP coaxial jet as a function of local shear layer half-width b: $fD_1/U_1 = 0{\cdot}2$. Calculated results using numerically generated mean flow: inner shear layer, ——, $n = 0$: ---, $n = 1$; outer shear layer, — — —, $n = 0$, — · — ·-, $n = 1$. Results from reference [16] mean flow defined by analytic functions: inner shear layer, ○, $n = 0$; □, $n = 1$; outer shear layer, ◇, $n = 0$, △, $n = 1$. (a) Phase velocity relative to ambient speed of sound; (b) growth rate.

TABLE 1

Operating conditions for the supersonic coaxial jet calculations

AR	r	s	U_1 (m/s)	U_2 (m/s)	T_1 (K)	T_2 (K)	M_1	M_2
Reference jet								
—	—	—	1330·0	—	1100·0	—	2·00	—
IVP jets								
1·25	1·25	0·60	1186·5	1483·1	845·0	1408·3	2·04	1·97
1·25	1·50	0·60	1051·6	1577·4	821·4	1369·1	1·83	2·13
1·25	2·00	0·60	831·3	1662·5	763·9	1273·1	1·50	2·32
1·25	2·50	0·60	672·3	1680·8	710·5	1184·2	1·26	2·44
1·25	2·00	0·40	886·7	1773·3	651·8	1629·6	1·73	2·19
1·25	2·00	0·50	855·0	1710·0	707·1	1414·3	1·60	2·27
1·25	2·00	0·70	812·8	1625·6	821·6	1173·7	1·41	2·37
1·00	2·00	0·60	860·6	1721·2	782·9	1304·9	1·53	2·38
0·75	2·00	0·60	902·5	1805·0	810·4	1350·7	1·58	2·45
0·50	2·00	0·60	967·3	1934·5	853·3	1422·2	1·65	2·56
0·50	1·25	0·40	1266·7	1583·3	873·0	2182·5	2·14	1·69

Area ratio $AR = A_2/A_1$; Velocity ratio $r = U_2/U_1$, density ratio $s = \rho_2/\rho_1 = T_1/T_2$, (constant thrust and constant mass flow).

3. NUMERICAL PREDICTIONS

The mean flow prediction scheme and the instability wave noise generation model were used to study the effect of changing various operating parameters on the instability wave noise generation from perfectly expanded, supersonic IVP coaxial jets. We chose the operating conditions to have the same total thrust, mass flow and exit area as a single reference jet using the formulations given in Dahl [18]. The values chosen for the present study are shown in Table 1, and the reason for choosing these values will be discussed later. The single reference jet had an exit velocity of 1330 m/s and an exit static temperature of 1100 K, resulting in an exit Mach number of 2. When scaled up, this jet would produce thrusts and mass flows comparable to those projected for supersonic jet transport aircraft engines.

3.1. STABILITY CHARACTERISTICS

The eigenvalues of the Rayleigh equation (2) were calculated for both shear layers at each axial location at which the mean flow profiles were calculated. The real and imaginary parts of the eigenvalues may be identified with the local phase velocities and growth rates of the instability wave. Typical calculated values are shown in Figure 2 for an IVP jet, where part (a) contains results for the axisymmetric ($n = 0$) mode and part (b) contains results for the first helical ($n = 1$) mode. The IVP jet had a velocity ratio of 2·0, a density ratio of 0·6 (indicating that the outer stream is hotter than the inner stream), and an area ratio of 1·25. The calculations were performed at four Strouhal numbers fD_e/U_e, where U_e and D_e are the exit velocity and diameter, respectively, of the reference jet and f is the cyclical frequency. This means that the calculations for each shear layer were performed at the same frequency. In the figure are indicated the axial location of the end of the outer potential core (where the two shear layers begin to merge), the axial location of the end of the inner potential core after which the centerline velocity typically increases as the higher speed outer stream spreads toward the axis, and the axial location at which the maximum jet velocity has reached the jet axis and the flow is fully merged. Also, an indication is given in the figure of the shear layer with which the stability characteristic

is initially associated (inner or outer) and the maximum amplitude the instability wave achieves relative to its initial amplitude. The maximum amplitude is calculated by

$$A_{max} = \left| \exp \int_0^{x_c} \alpha(\chi)\, \mathrm{d}\chi \right|, \tag{8}$$

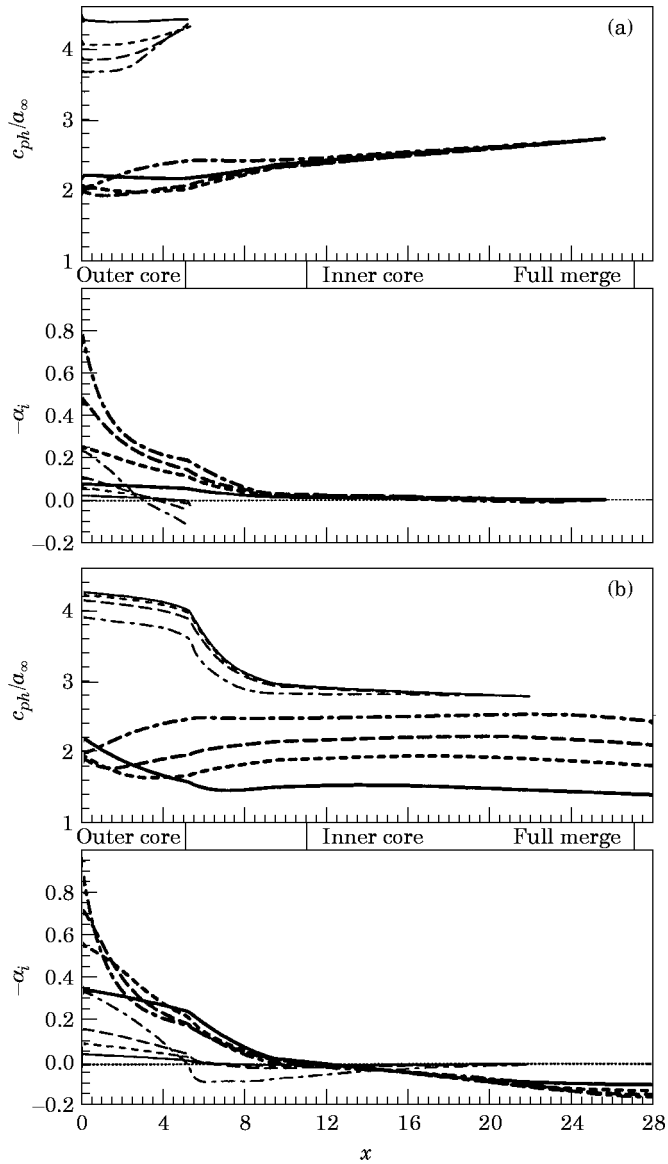

Figure 2. Growth rates and phase velocities relative to the ambient speed of sound for both shear layers of an IVP jet with $U_2/U_1 = 2{\cdot}0$, $\rho_2/\rho_1 = 0{\cdot}6$ and $AR = 1{\cdot}25$. The legend defined lines with numbered pairs (fD_e/U_e, maximum amplitude from equation (8)). (a) $n = 0$, inner shear layers: ——, 0·06, 1·077; ---, 0·12, 1·165; ——, 0·20, 1·256; — - — -, 0·40, 1·495. Outer shear layer: ——, 0·06, 1·900; - - -, 0·12, 3·987; ——, 0·20, 6·816; — - — -, 0·40, 9·568. (b) $n = 1$, inner shear layer: ——, 0·06, 1·221; ---, 0·12, 1·473; ——, 0·20, 1·854; — - — -, 0·40, 2·767. Outer shear layer: ——, 0·06, 8·588; - - -, 0·12, 11·996; ——, 0·20, 11·135; — - — -, 0·40, 9·316.

where x_c is the point at which α_i, the imaginary part of α, is zero. All of the stability characteristics shown are of the Kelvin–Helmholtz type, and all of the phase velocities shown are supersonic relative to the ambient speed of sound.

According to the mean flow model used in this study, when two shear layers of an IVP jet begin to merge after the end of the outer potential core, the rate of mixing increases in the jet, causing the jet to spread more rapidly than in the potential core region. As a shear layer spreads, it has less ability to sustain a growing instability wave and the wave decays with axial distance. If the inner shear layer instability waves have not begun to decay by the end of the outer potential core, their growth rate decreases rapidly after that point. Further downstream, as the maximum velocity moves toward the jet axis, the inner shear layer disappears along with any inviscid, inflectional, instability wave.

The outer shear layer always exists in an IVP jet and the stability calculations are made in the same manner as for a single jet. For an inviscid calculation, the outer shear layer $n = 0$ mode calculations are made until the phase speed approaches the maximum velocity in the mean flow profile. The calculations are not valid after that point. The growth rate plots in Figure 2(a) show that the $n = 0$ mode instability waves are slightly damped at the point where the calculation ends. For the outer shear layer $n = 1$ modes, the instability calculations are continued into the damped region using the contour path in the complex plane described in Part 2 of this paper [1]. As shown in Figure 2(b), these modes have much higher rates of damping than the $n = 0$ modes. For both modes, the growth rates decrease more rapidly after the end of the outer potential core. The instability waves peak as the growth rates go to zero after the inner potential core ends and they are decaying before the flow is fully merged. As listed in the figure, the relative maximum amplitudes for the outer shear layer instability waves are always larger than the inner shear layer amplitudes for the four Strouhal numbers used in the calculations. Furthermore, the $n = 1$ mode outer shear layer instability waves have typically higher amplitudes than the $n = 0$ mode instability waves except at $fD_e/U_e = 0{\cdot}4$, where the amplitudes are similar in level. Therefore, when we compare the effects of changes in operating conditions between different IVP jets and between the IVP jets and the reference jet, we will concentrate on results for the $n = 1$ mode instability waves in the outer shear layer.

In Figure 2, the inner shear layer instability wave growth rates are shown to be lower than the outer shear layer growth rates. This is due both to the fact that the inner shear layer is smaller than the outer shear layer and that the spreading of the high speed outer stream toward the jet axis is causing the inner shear layer to disappear. Despite this, the presence of the inner shear layer affects the local growth rates and phase velocities of the instability waves in the outer shear layer. To show this, we chose a single jet with operating conditions $U = 1552{\cdot}9$ m/s and $T = 937{\cdot}9$ K and a coaxial jet with the same outer stream conditions as the single jet and reduced the inner stream such that $U_2/U_1 = 2{\cdot}5$, $\rho_2/\rho_1 = 1{\cdot}02$ and $R_2/R_1 = 1{\cdot}5$. For this example, we did not maintain thrust and mass flow. However, the initial conditions and spreading rates for the outer shear layers were identical for the two jets. The resulting calculated stability characteristics for $fD/U = 0{\cdot}05$ are shown in Figure 3. Note that the jet shear layer half-width b is the same for the two jets out to the point at which the outer potential core ends for the coaxial jet. With the inner shear layer present, the local growth rates for the outer shear layer are larger than those for the single jet, even though the two shear layers have identical spreading characteristics. With the end of the outer potential core, we see from the half-width that the outer shear layer is spreading faster, causing the growth rate to decrease. This reduces the potential maximum amplitude of the instability wave if this growth rate decrease had not occurred. The presence of the inner shear layer has the added feature of reducing the local phase velocities of the outer shear layer. This condition was also measured in low speed jets [14].

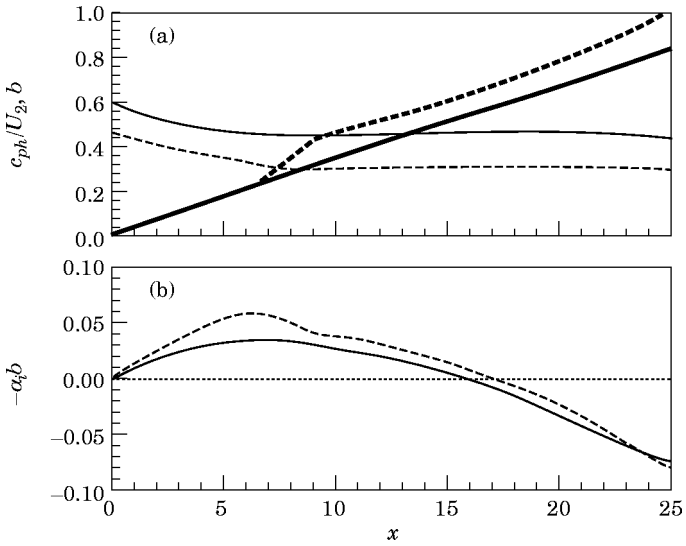

Figure 3. A comparison of growth rates and phase velocities between a single jet shear layer (jet exit diameter D and exit velocity U) and a coaxial IVP jet outer shear layer (outer jet exit diameter D_2 and exit velocity U_2, $U_2/U_1 = 2{\cdot}5$, $R_2/R_1 = 1{\cdot}5$) with the same flow conditions ($D = D_2$ and $U = U_2$): $n = 1$, $fD/U = 0{\cdot}05$. (a) Phase velocity: ——, for single jet shear layer relative to U; – – –, for IVP jet outer shear layer relative to U_2. Shear layer half-width b: ——, single jet shear layer; – – –, IVP outer shear layer. (b) Growth rates relative to shear layer half-width: ——, single jet shear layer; ——, IVP jet outer shear layer.

For fixed outer stream conditions, it was found that the outer shear layer growth rates increased and the phase velocities decreased as the inner shear layer velocity difference increased over the range $1 < U_2/U_1 \leqslant 2{\cdot}5$.

3.2. CHOICE OF OPERATING CONDITIONS

In an earlier study of IVP jets [19], the operating conditions were chosen to have the same thrust, mass flow and exit area as a single reference jet and to be constrained by the minimum noise condition [12]. The resulting far field directivity patterns showed relative peak levels that were much higher than those of the reference jet. When operating conditions were not constrained by minimum noise but chosen for any perfectly expanded jet [20], the relative far field peak levels were shown to be reduced by increasing the temperature of the high speed stream relative to the temperature of the low speed stream, decreasing the area ratio, and artificially increasing the initial spreading rate of the outer shear layer (simulating enhanced mixing). In many cases, the relative peak levels were still higher than those of the reference jet.

The far field peak levels are directly related to the maximum amplitude of a growing and decaying instability wave. Thus, in order to reduce far field peak levels, we need to reduce the maximum amplitude of the instability wave. In the outer shear layer of IVP jets, this amplitude is determined primarily by both the initial spreading rate of the outer shear layer and the length of the outer potential core. Both of these parameters are affected by the operating conditions. Since the effects of the end of the outer potential core are always beneficial in reducing the local growth rates of an instability wave and its length is affected by the outer shear layer spreading rate, the outer shear layer initial spreading rate is used as a parameter for choosing the jet operating conditions.

Using the definition for the vorticity thickness spreading rate δ'_ω given in Part 1 of this paper [2] and the equations that ensure that any coaxial jet operating conditions have the

same thrust, mass flow and exit area as a single reference jet [18], we determined the outer shear layer initial spreading rate as a function of the inner shear layer velocity ratio, the inner shear layer density ratio, and the area ratio. With the area ratio fixed at 1·25, a contour plot of δ'_ω as a function of the first two parameters is shown in Figure 4. We can consider the single reference jet as a special case of an IVP jet with velocity and density ratios equal to one. This point is located in the lower right corner. The initial spreading rate for the reference jet shear layer is approximately 0·06, and that contour is indicated by a heavy solid line. Above and to the right of this contour, the initial spreading rate for the outer shear layer is less than that of the reference jet shear layer. The outer shear initial spreading rate increases to the left and below the 0·06 contour. It is hypothesized that choosing operating conditions in this region will more likely result in lower instability wave maximum amplitudes and, hence, lower far field peak levels than other operating conditions. Centered about the operating condition with $U_2/U_1 = 2{\cdot}0$ and $\rho_2/\rho_1 = 0{\cdot}6$, we chose the conditions indicated by the points in Figure 4 to study the effects of variations with constant velocity ratio and with constant density ratio. In addition, the heavy dashed line shows the 0·06 contour for area ratio 0·5. In the δ'_ω region shown, the 0·06 contour shifts to the right as the area ratio decreases. Thus, for $U_2/U_1 = 2{\cdot}0$ and $\rho_2/\rho_1 = 0{\cdot}6$, the outer shear layer initial spreading rate will increase as the area ratio decreases. Additional operating conditions are chosen to examine the effect of area ratio changes. All of the operating conditions are shown in Table 1.

3.3. EFFECTS OF VELOCITY RATIO

The maximum amplitudes for the $n = 1$ instability waves in the outer shear layer are shown in Figure 5 as a function of the velocity ratio and the Strouhal number. Since the operating conditions were chosen based on the initial outer shear layer spreading rate, the IVP and reference jet results are placed in order of increasing spreading rate. Thus in accord with Figure 4, the reference jet maximum amplitudes are placed between the IVP jet results with $U_2/U_1 = 1{\cdot}50$ and with $U_2/U_1 = 2{\cdot}00$. As can be seen, the maximum

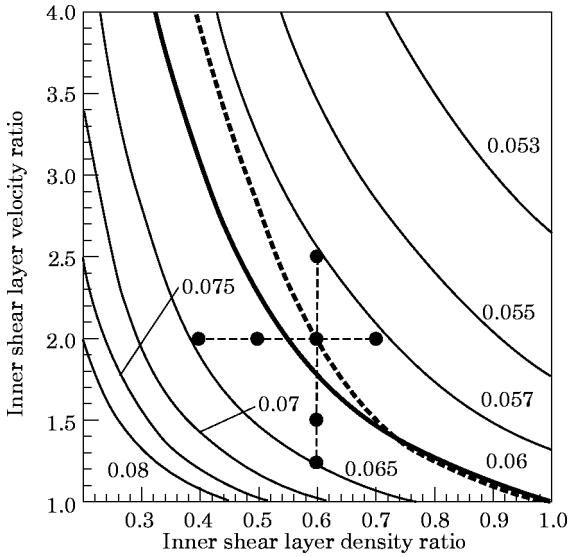

Figure 4. Contours of initial vorticity thickness spreading rates for the outer shear layer of IVP jets with $AR = 1{\cdot}25$. The heavy dashed line corresponds to $AR = 0{\cdot}5$. Single jet conditions are at the lower right. Points indicate operating conditions in Table 1.

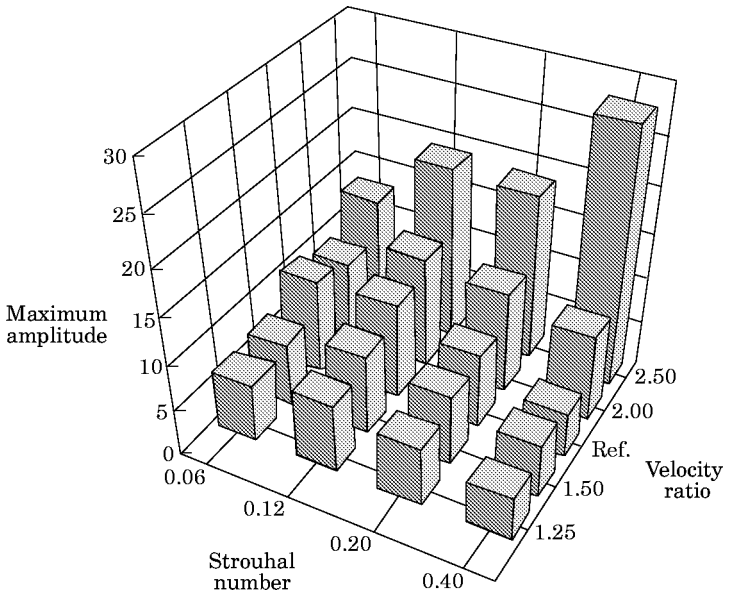

Figure 5. The effects of the velocity ratio and the Strouhal number on the maximum amplitude of instability waves in the outer shear layer: $n = 1$, $\rho_2/\rho_1 = 0{\cdot}6$, $AR = 1{\cdot}25$.

amplitudes increase for all Strouhal numbers as the velocity ratio increases for the IVP jets. Using the constant thrust, mass flow and exit area criteria, the following factors promote larger instability wave growth rates in the outer shear layer resulting in higher maximum amplitudes: increasing the outer stream velocity, increasing the inner shear layer ΔU and decreasing the outer shear layer spreading rate. The maximum amplitudes are also affected by the end of the outer potential core and this effect depends on the Strouhal number. At low Strouhal numbers, the growth rates are decreasing rapidly after the outer core ends, as shown in Figure 2. Thus, these IVP jet outer shear layer instability waves have lower maximum amplitudes than would be obtained for the reference jet shear layer with the same initial spreading rate. For high Strouhal numbers, most of the instability wave growth occurs in the core region. Consequently, the flow conditions for the IVP jets will promote higher maximum amplitudes when the outer shear layer spreading rate are comparable to that of the reference jet.

The far field directivity patterns for these velocity ratio effect cases are shown in Figure 6. As described in Part 2 of this paper [1], the far field directivity peak levels for the reference jet are set to an arbitrary level and all IVP jet results are referenced to the same level. This allows comparisons to be made of the relative changes in noise radiation between different Strouhal number instability waves and when operating conditions are changed. Relative to the single reference jet, the higher Strouhal number patterns for the IVP jet have higher relative levels than the lower Strouhal number patterns. This trend was observed by Tanna [10, 21] where shock-free IVP jets were noisier than the single reference jet at high frequencies and quieter at low frequencies. Also, the peak levels tend to become higher as the velocity ratio increases (initial outer shear layer spreading rate decreases), and since a larger velocity ratio increases the ΔU across the inner shear layer which decreases the local phase velocities of the outer shear instability waves, the directivity patterns shift toward lower angles.

3.4. EFFECTS OF DENSITY RATIO

In Figure 4 it is shown that we can also change the density ratio with the velocity ratio fixed in order to obtain an initial spreading rate of the outer shear layer of an IVP jet that is higher than the spreading rate of the reference jet shear layer. The calculated results for the instability wave maximum amplitudes are shown in Figure 7 as a function of the density ratio and the Strouhal number. The general trend again exists that as the spreading rate increases (lower density ratios) the maximum amplitudes decrease. In this case, these changes are governed more by the outer stream temperature than by velocity difference effects. This is especially true for the inner shear layer velocity difference, which changes very little when the density ratio is changed compared to the velocity ratio effect changes above. As the outer stream total temperature increases (the density ratio decreases), the maximum amplitudes decrease [22]. The conditions regarding the effects of the end of the outer potential core, as described above, still apply here, where the lower Strouhal number amplitudes are lower than the reference jet and the higher Strouhal number amplitudes are higher.

The far field directivity patterns are shown in Figure 8. As seen in Figure 6, there is an increase in higher Strouhal number peaks relative to lower Strouhal peaks when the IVP jet directivity patterns are compared to the reference jet directivity patterns. However, little change is seen in the relative peak levels for the IVP jets as the density ratio is changed

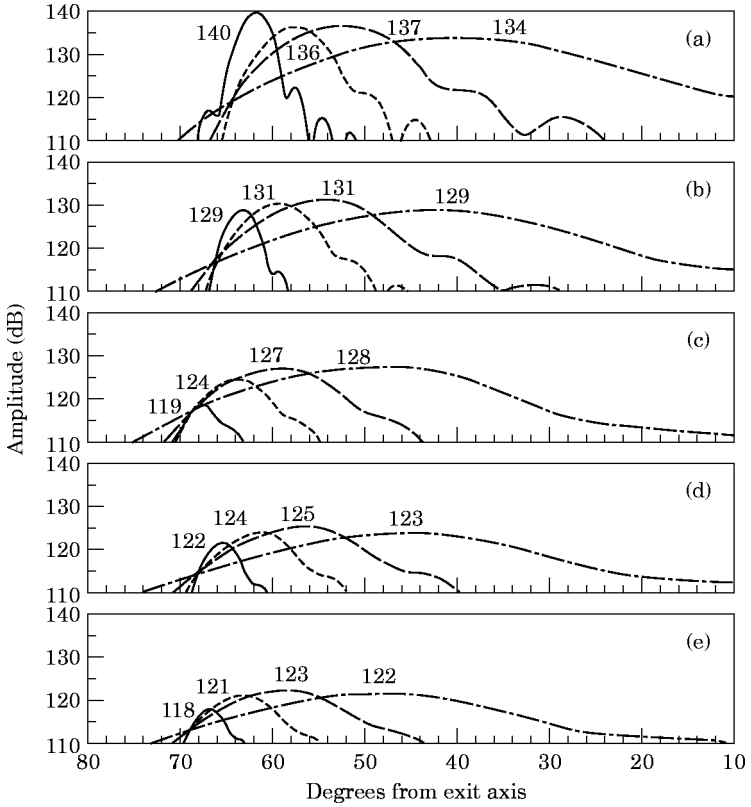

Figure 6. The effects of the velocity ratio on the far field directivity patterns for noise radiated from instability waves in the outer shear layer. Numbers indicate peak amplitudes: $n = 1$, $\rho_2/\rho_1 = 0{\cdot}6$, $AR = 1{\cdot}25$. IVP jet with $U_2/U_1 =$ (a) 2·50, (b) 2·00, (d) 1·50 and (e) 1·25. (c) Reference jet. Strouhal number: — - — -, 0·06; ——, 0·12; ---, 0·20; ——, 0·40.

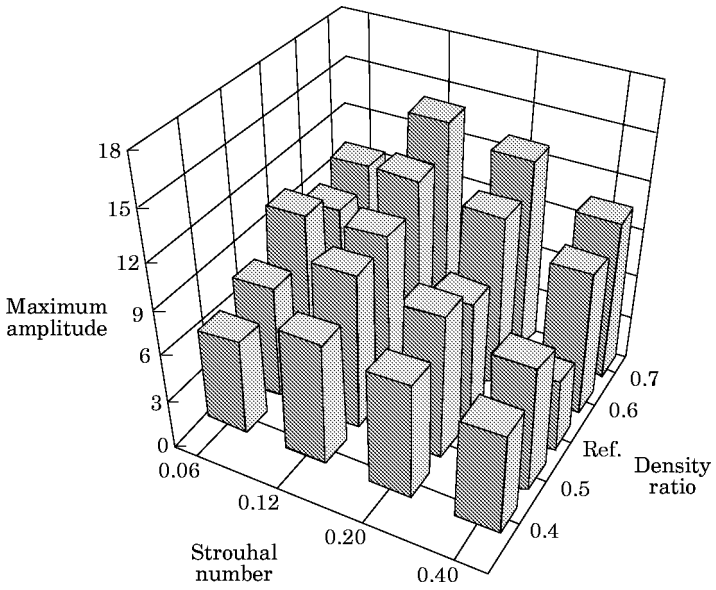

Figure 7. The effects of the density ratio and the Strouhal number on the maximum amplitude of instability waves in the outer shear layer: $n = 1$, $U_2/U_1 = 2{\cdot}0$, $AR = 1{\cdot}25$.

and little change in the peak directions. There is the general trend again toward reduced far field peak levels as the speading rate is increased for the outer shear, resulting from a decrease in the density ratio.

3.5. EFFECTS OF AREA RATIO

Decreasing the area ratio of an IVP jet decreases the length of the outer potential core even though the outer stream velocity must increase to maintain constant thrust and mass flow. With the two shear layers merging sooner, the instability wave growth rates in the outer shear layer are diminished sooner, as seen in Figure 9. For both Strouhal number 0·06 and 0·4 instability waves, the local growth rates decrease more rapidly after the end of the outer potential core and the instability waves become damped sooner as the merging mean flow spreads. The resulting far field noise radiation patterns are shown in Figure 10. The relative peak levels are decreasing with a smaller area ratio, with more reduction at lower Strouhal numbers than at higher Strouhal numbers.

3.6. COMBINED EFFECTS

The calculated results have shown that lower instability wave maximum amplitudes and lower relative far field noise peak levels are achieved when the velocity ratio, the density ratio and the area ratio are each decreased separately. This is illustrated in Figure 11, using far field directivity patterns for comparison. The base IVP jet operating parameters are given by $U_2/U_1 = 2{\cdot}0$, $\rho_2/\rho_1 = 0{\cdot}6$, and $AR = 1{\cdot}25$. As each individual parameter is reduced, the relative peak levels are reduced. When the IVP jet operating conditions are changed to the combined reduced condition of $U_2/U_1 = 1{\cdot}25$, $\rho_2/\rho_1 = 0{\cdot}4$ and $AR = 0{\cdot}5$, the far field peak levels are reduced further. The amount of reduction from the base condition levels for each Strouhal number is within 1·5 dB of the sum of the reductions for each parameter individually.

Another view of these results is to consider them with regard to the initial spreading rate of the outer shear layer. As shown in Figure 4, reducing each parameter separately

from the base conditions increases the outer shear layer initial spreading rate. This results in lower instability wave maximum amplitudes and, hence, less radiated noise. By combining parametric effects, we have moved to the lower left of Figure 4 and toward larger spreading rates as the area ratio is reduced. Compared to the base IVP jet with an outer shear layer spreading rate of 0·0589, the combined IVP jet spreading rate is 0·0806. This 37% increase in spreading rate results in the lower relative far field peak levels shown in Figure 11.

4. CONCLUSIONS

Linear instability wave analysis has been applied to the study of noise generation from growing and decaying instability waves in IVP supersonic coaxial jets. Even though the IVP jet had two shear layers initially, the instability waves in the outer shear layer were found to have larger growth rates and higher maximum amplitudes than the inner shear layer instability waves. As a result, they were the dominant generators of mixing noise in the downstream arc from a supersonic IVP jet. While the inner shear layer instability waves were ignored as noise generators, the presence of the inner shear layer had the following effects on the outer shear layer instability waves:

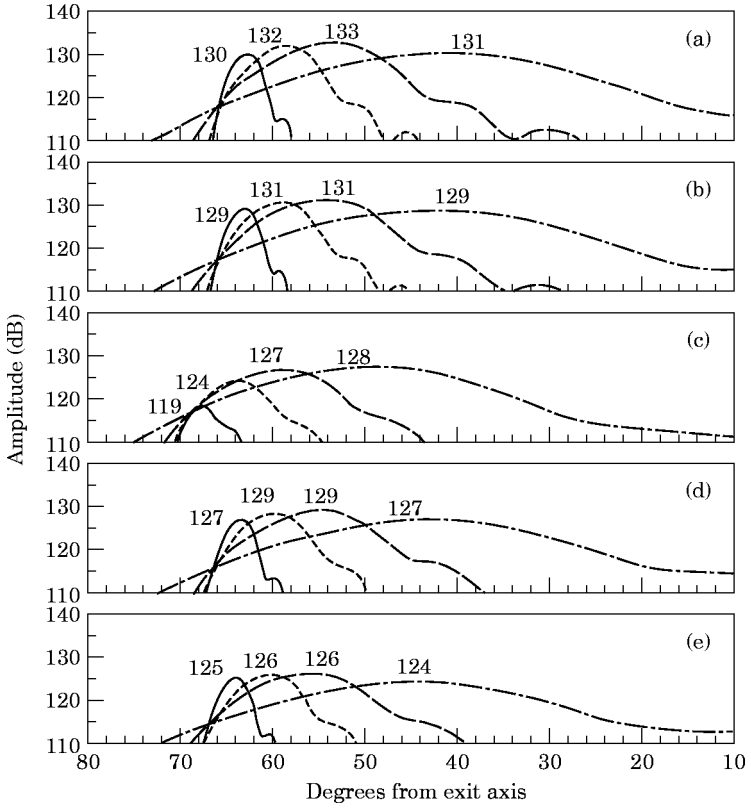

Figure 8. The effects of the density ratio on the far field directivity patterns for noise radiated from instability waves in the outer shear layer. Numbers indicate peak amplitudes: $n = 1$, $U_2/U_1 = 2{\cdot}0$, $AR = 1{\cdot}25$. IVP jet with $\rho_2/\rho_1 =$ (a) 0·7, (b) 0·6, (d) 0·5 and (e) 0·4. (c) Reference jet. Strouhal number: — - — -, 0·06; ——, 0·12; ---, 0·20; ——, 0·40.

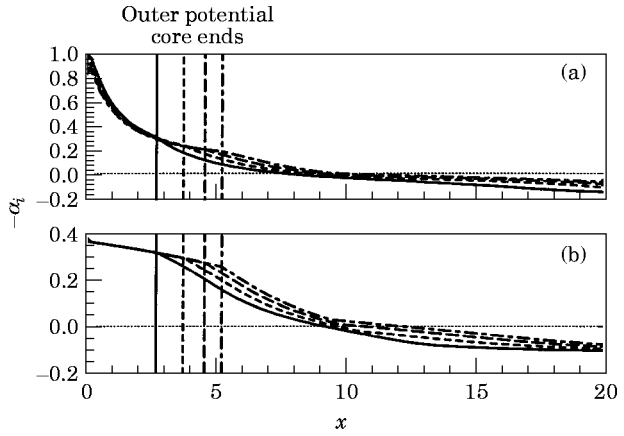

Figure 9. Instability wave local growth rates for IVP jets with a varying area ratio: $n = 1$, $U_2/U_1 = 2{\cdot}0$, $\rho_2/\rho_1 = 0{\cdot}6$, outer shear layer. Area ratio: — - — -, 1·25; – – –, 1·00; ---, 0·75; ——, 0·50. Strouhal number: (a) 0·40; (b) 0·06.

(1) For the same mean flow conditions and shear layer spreading rates, the presence of the inner shear layer resulted in the outer shear layer stability characteristics having higher growth rates and lower phase velocities than the single jet shear layer.

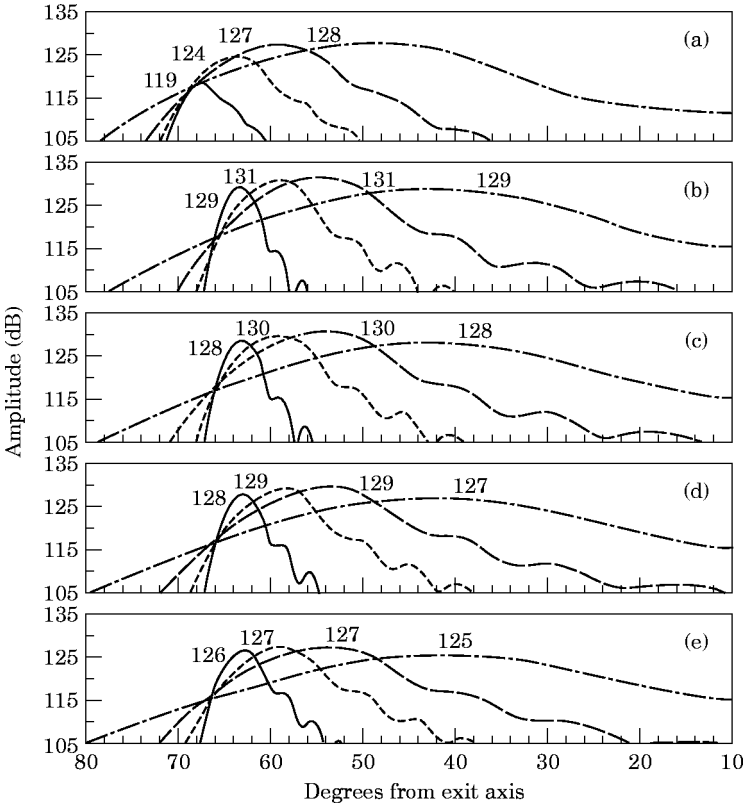

Figure 10. Far field directivity patterns for IVP jets with a varying area ratio: $n = 1$, $U_2/U_1 = 2{\cdot}0$, $\rho_2/\rho_1 = 0{\cdot}6$, outer shear layer. Numbers indicate peak amplitudes. (a) Reference jet. The area ratio is (b) 1·25, (c) 1·00, (d) 0·75 and (e) 0·50. Strouhal numbers: — - — -, 0·06; – – –, 0·12; ---, 0·20; ——, 0·40.

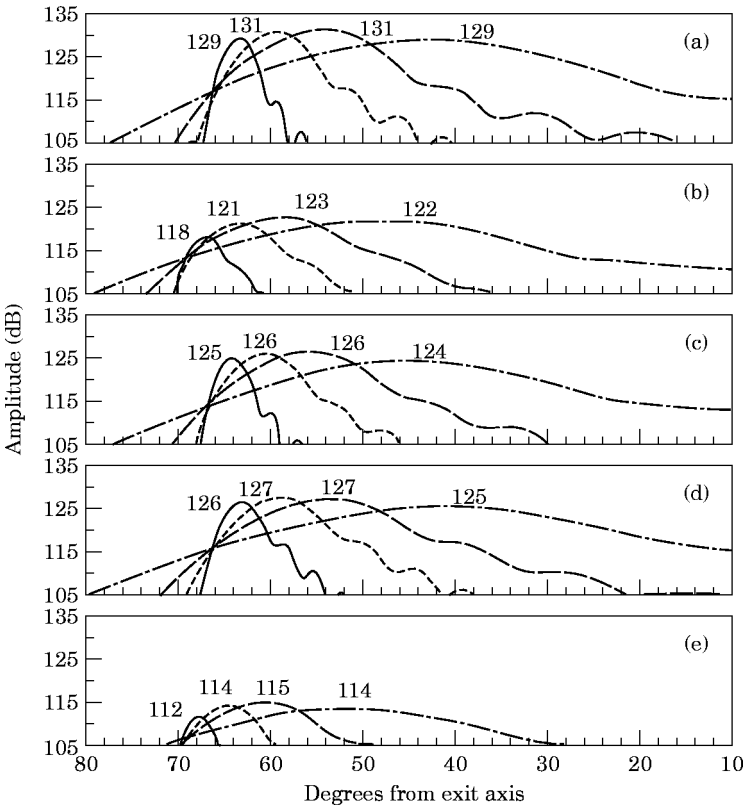

Figure 11. Far field directivity patterns for IVP jets comparing one parameter and combined parameter effects. (a) Base IVP jet parameters: $U_2/U_1 = 2{\cdot}0$, $\rho_2/\rho_1 = 0{\cdot}6$, $AR = 1{\cdot}25$. (b) Change velocity ratio $U_2/U_1 = 1{\cdot}25$. (c) Change density ratio $\rho_2/\rho_1 = 0{\cdot}4$. (d) Change area ratio $AR = 0{\cdot}5$. (e) Combined parameters: $U_2/U_1 = 1{\cdot}25$, $\rho_2/\rho_1 = 0{\cdot}4$, $AR = 0{\cdot}5$. $n = 1$, outer shear layer. Numbers indicate peak amplitudes. Strouhal numbers: — · — ·, 0·06; – – –, 0·12; ---, 0·20; ——, 0·40.

(2) Along with the spreading outer shear layer, the spreading inner shear layer created a separate outer stream potential core. After this potential core ended, the outer shear layer instability wave growth rates decreased due to increased jet spreading. This lowered the potential maximum amplitude of the instability waves. The maximum amplitude decreased with shorter potential core lengths.

A parametric study of the effects of various operating conditions was conducted using the conditions that the IVP jets had the same total thrust, mass flow and exit area as a single reference jet. The choice of operating conditions was based on an analysis of outer shear layer spreading rates. It was proposed that the IVP jets with outer shear layer spreading rates higher than the reference jet spreading rate would be beneficial in reducing the maximum amplitudes of the instability waves and thus lower radiated noise levels. The analysis identified regions of higher and lower spreading rates and operating conditions were chosen in both regions to study the changes that occurred as a function of the velocity ratio, the density ratio and the area ratio between the outer and inner flow streams. The following results were found:

(1) Operating conditions in the region of higher outer shear layer spreading rates were a necessary condition to achieve generally lower maximum instability wave amplitudes and less relative radiated noise levels than the reference jet. However, amplitudes were

dependent on the Strouhal number and could be higher or lower than the reference jet amplitudes. In the lower spreading rate region, the amplitudes were mostly higher.

(2) Lower Strouhal number instability waves were particularly affected by the end of the outer potential core. The growth rate decreased after that point, lowering the potential maximum amplitude.

(3) Higher Strouhal number instability waves had their primary growth within the core region. Thus, initial flow conditions governed the growth rates of these waves, which often resulted in their having higher relative amplitudes than the reference jet amplitudes.

(4) The supersonic IVP jet can radiate less mixing noise than the reference jet if the velocity ratio is small, the outer stream is hotter than the inner stream, and the area ratio is small. The operating conditions to achieve this are found from an analysis of shear layer spreading rates, as shown in Figure 4, where the outer shear layer initial spreading rate is higher than the initial spreading rate of the reference jet.

REFERENCES

1. M. D. Dahl and P. J. Morris 1997 *Journal of Sound and Vibration* **200**, 665–699. Noise from supersonic coaxial jets, part 2: normal velocity profile.
2. M. D. Dahl and P. J. Morris 1997 *Journal of Sound and Vibration* **200**, 643–663. Noise from supersonic coaxial jets, part 1: mean flow predictions.
3. T. J. Williams, M. R. M. H. Ali and J. S. Anderson 1969 *Journal of Mechanical Engineering Science* **11**, 133–142. Noise and flow characteristics of coaxial jets.
4. D. S. Dosanjh, A. N. Abdelhamid and J. C. Yu 1969 *Basic Aerodynamic Noise Research*, *NASA SP*-207, 63–101. Noise reduction from interacting coaxial supersonic jet flows.
5. D. S. Dosanjh, J. C. Yu and A. N. Abdelhamid 1970 *AIAA Paper No*. 70–236. Reduction of noise from supersonic jet flows.
6. J. C. Yu and D. S. Dosanjh 1971 *AIAA Paper No*. 71–152. Noise field of coaxial interacting supersonic jet flows.
7. K. K. Ahuja 1976 *Ph.D. Dissertation*, *Syracuse University*. Noise studies of cold and heated model jets at supersonic and high subsonic speeds with particular reference to noise reduction.
8. M. R. Bassiouni 1976 *Ph.D. Dissertation*, *Syracuse University*. Acoustic and flow characteristics of cold high-speed coaxial jets.
9. P. K. Bhutiani 1976 *Ph.D. Dissertation*, *Syracuse University*. Investigations of the radiated noise from coaxial supersonic jets to study: I, the effect of heating one of the jets; II, the role of lip thickness on noise suppression.
10. H. K. Tanna, B. J. Tester and J. C. Lau 1979 *NASA CR*-158995. The noise and flow characteristics of inverted-profile coannular jets.
11. J. R. Maus, B. H. Goethert and C. V. Sundaram 1980 *AIAA Paper No*. 80–0167. Noise characteristics of coannular flows with conventional and inverted velocity profiles.
12. H. K. Tanna, W. H. Brown and C. K. W. Tam 1985 *Journal of Sound and Vibration* **98**, 95–113. Shock associated noise of inverted-profile coannular jets, part I: experiments.
13. N. W. M. Ko and H. Au 1985 *Journal of Sound and Vibration* **100**, 211–232. Coaxial jets of different mean velocity ratios.
14. H. Au and N. W. M. Ko 1987 *Journal of Sound and Vibration* **116**, 427–443. Coaxial jets of different mean velocity ratios, part 2.
15. W. J. A. Dahm, C. E. Frieler and G. Tryggvason 1992 *Journal of Fluid Mechanics* **241**, 371–402. Vortex structure and dynamics in the near field of a coaxial jet.
16. T. R. S. Bhat and J. M. Seiner 1993 *AIAA Paper No*. 93–4410. The effect of velocity profiles on supersonic jet noise.
17. C. K. W. Tam and D. E. Burton 1984 *Journal of Fluid Mechanics* **138**, 273–295. Sound generated by instability waves of supersonic flows, part 2: axisymmetric jets.
18. M. D. Dahl 1994 *Ph.D. Dissertation*, *Penn State University*. The aeroacoustics of supersonic coaxial jets.
19. M. D. Dahl and P. J. Morris 1994 *AIAA Paper No*. 94–2190. Noise radiation by instability waves in coaxial jets.

20. M. D. Dahl and P. J. Morris 1995 *CEAS/AIAA Paper No*. 95–171. Supersonic coaxial jet noise predictions.
21. H. K. Tanna 1980 *Journal of Sound and Vibration* **72**, 97–118. Coannular jets—are they really quiet and why?
22. J. M. Seiner, T. R. S. Bhat and M. K. Ponton 1993 *AIAA Paper No*. 93–0734. Mach wave emission from a high temperature supersonic jet.